Electronic band gap and transport in graphene superlattice with a Gaussian profile potential voltage*

Zhang Yu-Ping(张玉萍)†, Yin Yi-Heng(尹贻恒), Lü Huan-Huan(吕欢欢), and Zhang Hui-Yun(张会云)

Qingdao Key Laboratory of Terahertz Technology, College of Science, Shandong University of Science and Technology, Qingdao 266510, *China*

(Received 9 August 2013; revised manuscript received 29 October 2013; published online 20 December 2013)

We study the electronic properties for the graphene-based one-dimensional superlattices, whose potential voltages vary according to the envelope of a Gaussian function. It is found that an unusual Dirac point exists and its location is exactly associated with a zero-averaged wave number (zero-$\bar{k}$) gap. This zero-$\bar{k}$ gap is less sensitive to incident angle and lattice constants, properties opposing those of Bragg gap. The defect mode appearing inside the zero-$\bar{k}$ gap has an effect on transmission, conductance, and shot noise, which will be useful for further investigation.

Keywords: graphene superlattice, Gaussian profile, energy band

PACS: 72.10.–d, 73.20.At, 73.23.–b, 73.22.–f **DOI:** 10.1088/1674-1056/23/2/027202

1. Introduction

Graphene is a two-dimensional stable single layer of carbon atoms densely packed in a honeycomb lattice. It has attracted considerable attention, owing to the intriguing physics as well as the applications in graphene-based nanoeletronics.[1–4] In graphene, low-energy charge carriers are formally described by a massless Dirac equation because of the conductance and valance bands touching at Dirac point (DP). This particular band structure leads to many unusual properties, such as ballistic conduction,[5] gate-tunable optical transition,[6] linear energy dispersion, half-integer quantum Hall effect,[7,8] frequency-dependent conductivity,[9] etc.

Recently, there have been a number of theoretical investigations on the new Dirac point in the band structure of the graphene superlattice (GSL) with periodic potential structures.[10–16] This new DP, associated with zero-averaged wave number zero-$\bar{k}$ gap,[17] is of benefit to the controllability of electronic transport. Different from Bragg gaps, the zero-$\bar{k}$ gap associated with the new DP is insensitive to lattice constant, structural disorder,[18] and an external magnetic field.[19] Furthermore, electronic transports in Fibonacci, Thue–Morse, and Double-periodic GSLs have been predicted, and the zero-$\bar{k}$ gap is found to exist in each of these quasi-periodic GSLs.[20–22] Yan[23] focused on the study of GSLs driven by linear potentials and demonstrated that the transmission shows the irrelevance to the number of periods. Additionally, the spin transport properties of a zigzag graphene superlattice have been investigated and it is found that the spin-polarized transport can be tuned through the variation of electron energy.[24]

In this paper, we investigate the electronic band gaps and transports in the graphene-based superlattices, with electric potentials varying according to the envelope of a Gaussian function. We find that zero-$\bar{k}$ gap occurs in each of these sequences, which results in the robust transmission property, conductance and short noise at the DP.

2. Model and formulation

Figure 1 shows the basic idea of the structures studied in this work. They consist of a periodic repetition of a unit cell composed of two parts: A and B. Part A is composed of 21 layers with the same width w_A and electric potentials whose envelope varies as a Gaussian function. Part B is a single layer with a fixed width w_B and electric potential $V_B = 10$ meV. The potentials in part A vary from $V_1 = 10.88$ meV to a maximum value of $V_{11} = 29.95$ meV (for the 11th layer), which comes back to V_1, for the 21st layer. The combination of parts A and B makes a unit cell. In this paper, one complete superlattice is composed of 20 unit cells. We define a filling fraction $f = w_A/(w_A + w_B)$ with value changing from 0.1 to 0.9 and investigate its influence on transport properties.

In the presence of a potential $V(x)$, the Hamiltonian of charge carriers near the K point is described by the Dirac-like equation, $\hat{H} = \upsilon_F \hat{\sigma} \cdot \hat{p} + V(x)\hat{I}$, where

$$\boldsymbol{p} = (p_x, p_y) = \left(-\mathrm{i}\hbar\frac{\partial}{\partial x}, -\mathrm{i}\hbar\frac{\partial}{\partial y}\right)$$

*Project supported by the National Natural Science Foundation of China (Grant No. 61001018), the Natural Science Foundation of Shandong Province, China (Grant Nos. ZR2011FM009 and ZR2012FM011), the Research Fund of Shandong University of Science and Technology, China (Grant Nos. 2010KYJQ103 and 2012KYTD103), the Project of Shandong Province Higher Educational Science and Technology Program, China (Grant No. J11LG20), the Qingdao Municipal Science & Technology Project, China (Grant No. 11-2-4-4-(8)-jch), the Qingdao Municipal Economic and Technical Development Zone Science and Technology Project, China (Grant No. 2013-1-64), and the Shandong University of Science and Technology Foundation, China (Grant No. YC130220).

†Corresponding author. E-mail: sdust_thz@163.com

© 2014 Chinese Physical Society and IOP Publishing Ltd

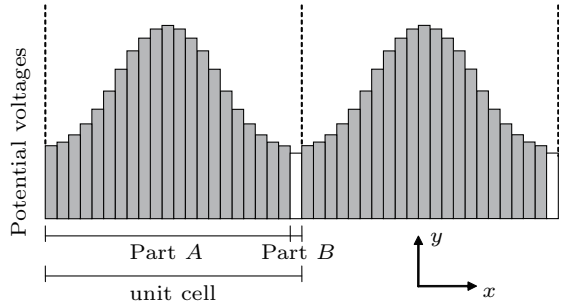


Fig. 1. Schematic diagram of the potential voltage profile of two unit cells corresponding to the typical superlattice structure studied in this work. Part A consists of 21 layers with the same width w_A, and with potential voltages adjusted to the envelope of a Gaussian function. The potential voltage in part A varies from $V_{\min} = 10.87$ meV to $V_{\max} = 29.95$ meV. Part B has a width w_B and a constant potential voltage $V_B = 10$ meV. Each unit cell is separated by a dashed line.

is the momentum operator with two components, $\hat{\sigma} = (\hat{\sigma}_x, \hat{\sigma}_y)$ are Pauli matrices, $\upsilon_F \approx 10^6$ m/s is the Fermi velocity, and $\hat{I}$ is a 2×2 unit matrix. The solution of the above equation for a given incident energy E and potential barrier V acting on the electronic pseudospin wavefunctions, leads to a transfer matrix[17]

$$M_j(\Delta x, E, k_y) = \begin{pmatrix} \dfrac{\cos(q_j\Delta x - \theta_j)}{\cos\theta_j} & \mathrm{i}\dfrac{\sin(q_j\Delta x)}{\cos\theta_j} \\ \mathrm{i}\dfrac{\sin(q_j\Delta x)}{\cos\theta_j} & \dfrac{\cos(q_j\Delta x + \theta_j)}{\cos\theta_j} \end{pmatrix}, \quad (1)$$

which connects the wave functions at any two positions x and $x + \Delta x$ inside the j-th potential with $\theta_j = \arcsin(k_y/k_j)$. Here, $q_j = \mathrm{sign}(k_j)\sqrt{k_j^2 - k_y^2}$ for $k_j^2 > k_y^2$, otherwise $q_j = \mathrm{i}\sqrt{k_y^2 - k_j^2}$, and k_y is the y component of k_j. As a consequence, the transmission coefficient $t(E, k_y)$ in such a device is found to be[17]

$$t(E, k_y) = \frac{2\cos\theta_0}{x_{22}\,\mathrm{e}^{-\mathrm{i}\theta_0} + x_{11}\,\mathrm{e}^{\mathrm{i}\theta_e} - x_{12}\,\mathrm{e}^{\mathrm{i}(\theta_e - \theta_0)} - x_{21}}, \quad (2)$$

where θ_0 and θ_e are incidence and exit angles, x_{ij} $(i, j = 1, 2)$ is the matrix element of total transfer matrix $X_n = (M_A M_B)^n$ which connects the incident and exit ends, with $M_A = M_1 \times M_2 \times \cdots M_{20} \times M_{21}$ and $n = 20$.

3. Results and discussion

Figure 2 shows the energy band structures with different values of w_A and f for the superlattice depicted in Fig. 1. We take $f = 1/2$ in Figs. 2(a) and 2(b), and $f = 1/5$ in Figs. 2(c) and 2(d), and $w_A = 10$ nm in Figs. 2(a) and 2(c) and $w_A = 20$ nm in Figs. 2(b) and 2(d), respectively. It is obvious that a band gap opens exactly at $E = 19$ meV under incident angle θ_0 as shown in Figs. 2(a) and 2(b). What is more, the upper and lower bands touch together and form a new cone Dirac point whose location is exactly at

$$\bar{k} = \sum_{j=1}^{N} k_j w_j \Big/ \sum_{j=1}^{N} w_j = 0. \quad (3)$$

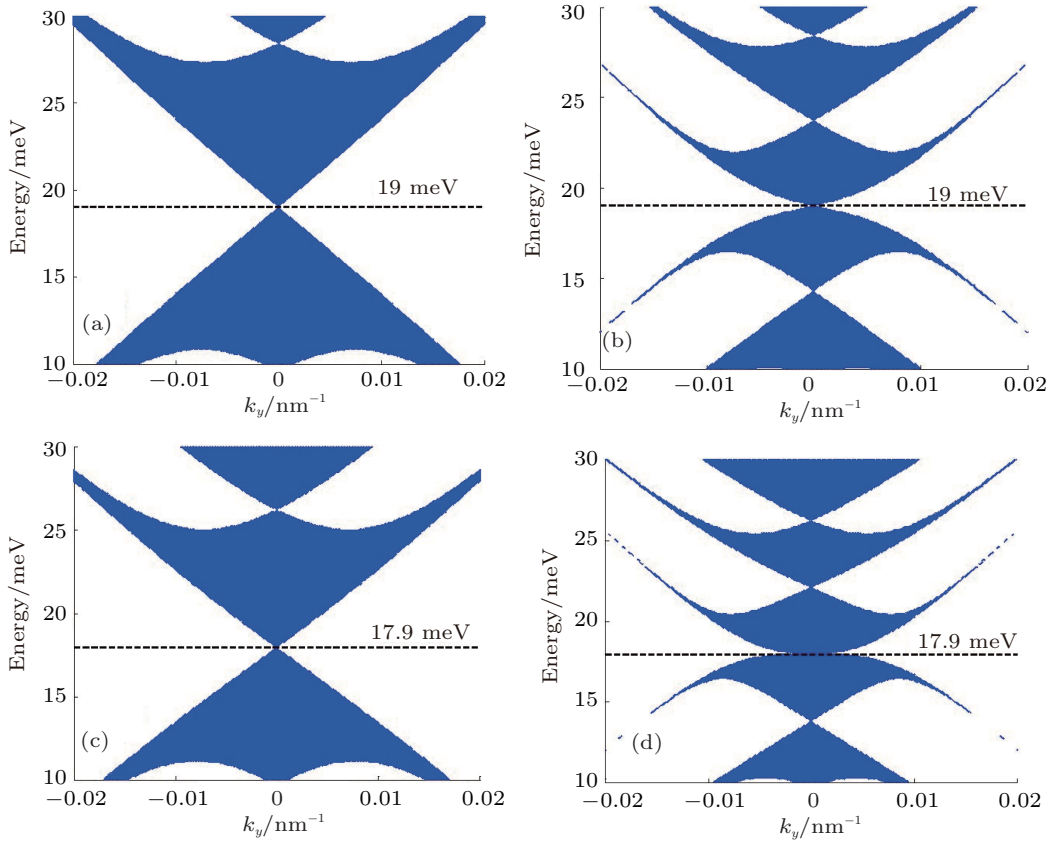


Fig. 2. (color online) Band structures for GSL, $(AB)^{20}$, where $V_B = 10$ meV and (a) $w_A = w_B = 10$ nm, (b) $w_A = w_B = 20$ nm, (c) $4w_A = w_B = 40$ nm, (d) $4w_A = w_B = 80$ nm. The horizontal dashed line denotes the new Dirac point's location.

It is easy to obtain the energy for $\bar{k}=0$ as follows:

$$E=\frac{f}{20f+1}\left(V_1+V_2+\cdots+V_{21}+\frac{1-f}{f}V_B\right), \qquad (4)$$

where $f=w_A/(w_A+w_B)$. As a matter of fact, in pristine graphene sheets, conduction and valence bands meet at $E=0$ and form a Dirac point. However, this point shifts to a new position in the GSL and possesses new characteristics, so we call it the new Dirac point. The position of the gap is exactly located at the zero average k which is indicated by a dashed line in Fig. 2, and we may call it zero-$\bar{k}$ gap. According to Eq. (4), the position of the DP is not shifted with lattice constant itself, but is shifted with the ratio f, which can also be seen in Fig. 3. We have $E=19$ meV for $f=1/2$, and $E=17.9$ meV for $f=1/5$ as shown in Figs. 2 and 3. From the point of view of application, this provides the possibility to control the electron transport by adjusting the ratio of lattice constants f.

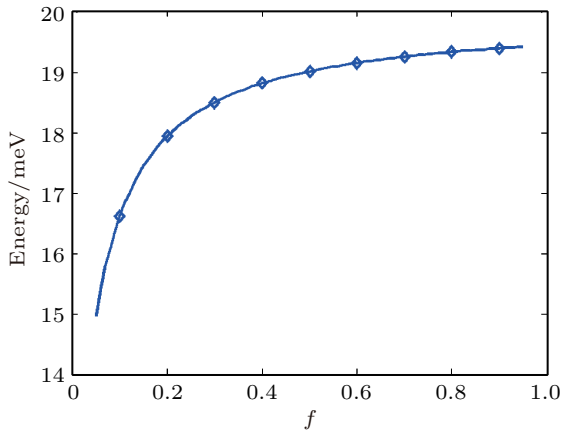


Fig. 3. (color online) The energy gap as a function of filling fraction f obtained from Eq. (4).

In Fig. 4(a), we calculate the transmission spectra for different lattice constants. It is obvious that the zero-$\bar{k}$ gap is insensitive to the lattice constants themselves. However, with the increase of lattice parameters, several other gaps emerge and their positions change sensitively. The influences of the incident angle, θ_0, on the transmission spectrum are also studied. Obviously, the zero-$\bar{k}$ gap associated with the Dirac point is insensitive to the incident angle as shown in Fig. 4(b). These properties of electronic transmission show significant differences from the conclusions drawn from GSLs driven by period linear potentials.

The total conductance G[25] and the Fano factor F[26] are also calculated, which are given by

$$G=G_0\int_0^{\pi/2}T\cos\theta_0\,\mathrm{d}\theta_0$$

and

$$F=\int_{-\pi/2}^{\pi/2}T(1-T)\cos\theta_0\,\mathrm{d}\theta_0\Big/\int_{-\pi/2}^{\pi/2}T\cos\theta_0\,\mathrm{d}\theta_0,$$

where $T=|t|^2$ and $G_0=2e^2mv_{\mathrm{F}}L_y/\hbar^2$ and L_y is the width of the graphene stripe in the y direction. The total conductance and the Fano factor, each as a function of incident energy with different lattice constants, are presented in Fig. 5. Obviously, the angular-averaged conductance reaches a minimum value at the DP, and F at the DP location presents a peak with a value of approximately 1/3.[19] From Fig. 5, we also find that the conductance and the Fano factor shift with the ratio of w_A/w_B, since the DP location depends on this ratio. Consequently, it can be inferred that the conductance of the GSL sequence could be verified by the ratio f.

Finally, we further shed light on the effect of the localized defect mode in the GSL, $(AB)^{10}D(AB)^{10}$, where the defect layer D has $w_D=50$ nm and $V_D=50$ meV. A comparison between Figs. 4 and 5 shows that the defect mode inside the zero-$\bar{k}$ gap is insensitive to incident angle and lattice constant while other defect modes greatly depend on these parameters. As shown in Fig. 6, the conductance is enhanced while the Fano factor is strongly suppressed. This suggests that the defect mode can modulate the electron transport.

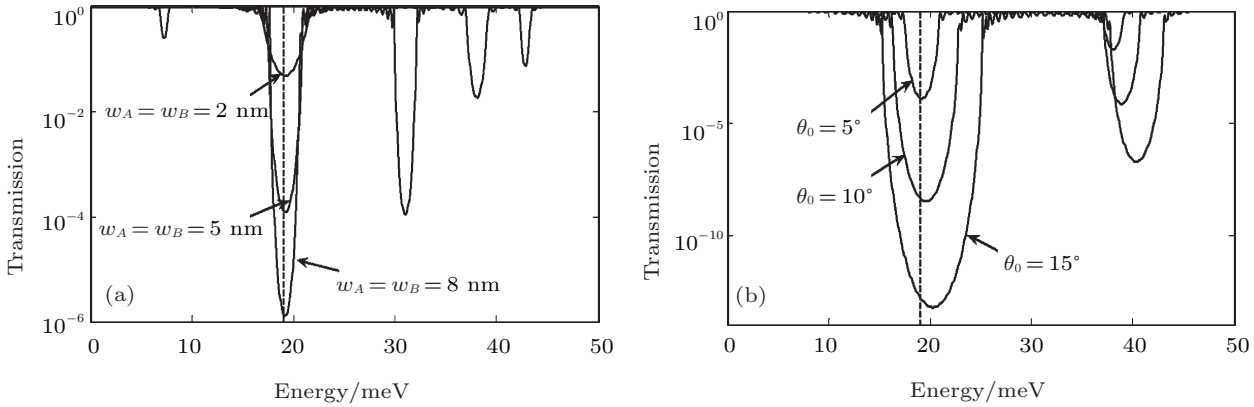


Fig. 4. (a) Dependences of transmission spectrum on width of potential barrier with incident angle $\theta_0=5°$; (b) energy-dependent transmission spectra at different incident angles with a fixed lattice constants $w_A=w_B=5$ nm. Other parameters are the same as those in Fig. 2.

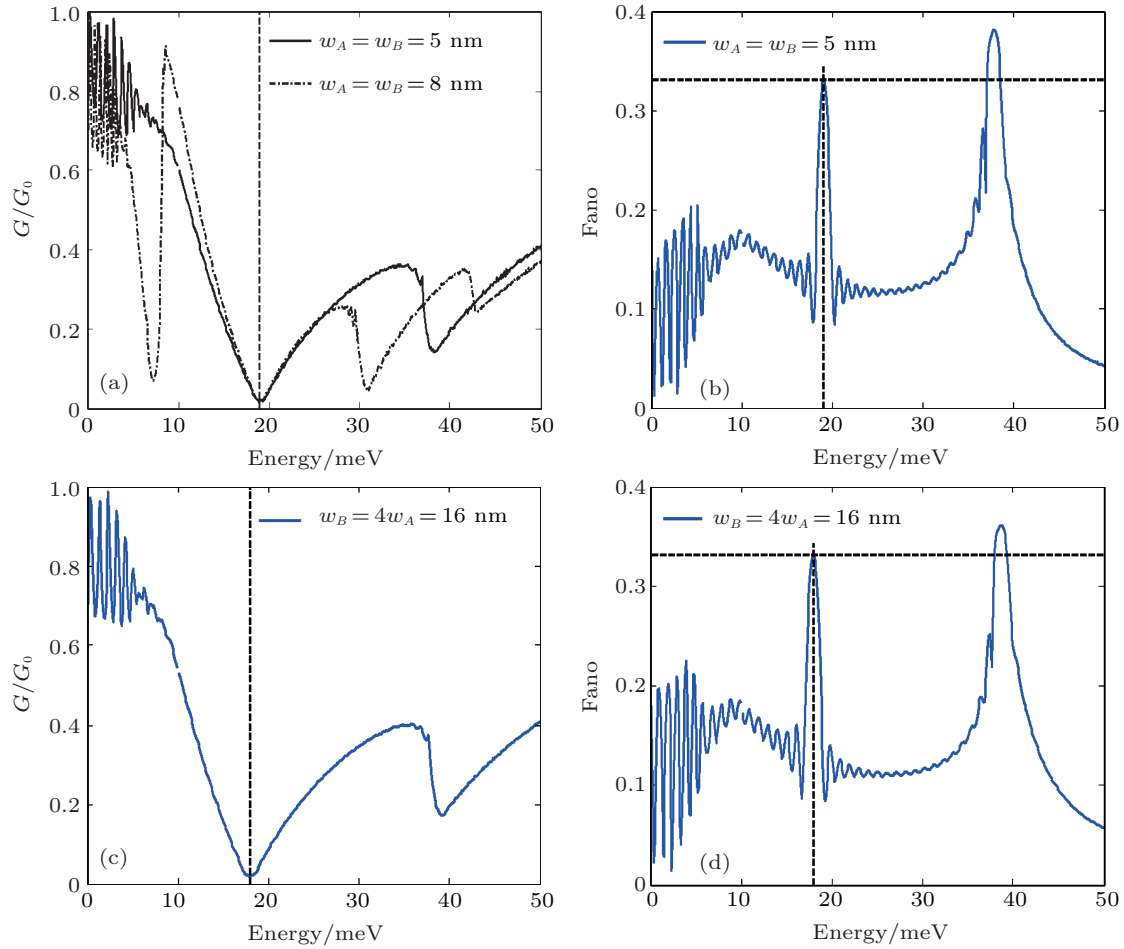


Fig. 5. (color online) Plots of conductance [(a) and (c)] and Fano factor [(b) and (d)] versus incident energy in the GSL sequence. Other parameters are the same as those in Fig. 2.

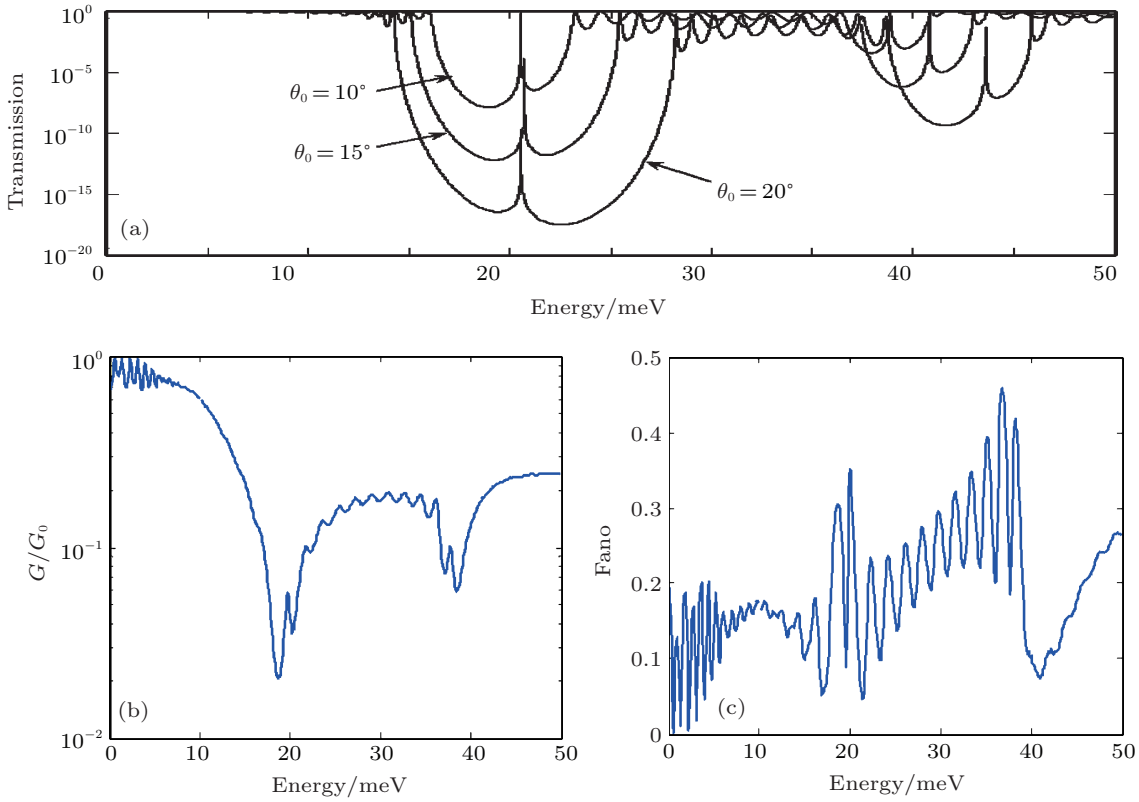


Fig. 6. (color online) Effects of defect mode on (a) transmission, (b) conductance, and (c) Fano factor in the GSL, where the defect $w_D = 50$ nm, $V_D = 50$ meV, $w_A = w_B = 5$ nm. Other parameters are the same as those in Fig. 2.

4. Conclusion

In this paper, we investigate the electronic band gap and transport properties in the GSL, consisting of multilayer with Gaussian profile potential voltages. It is found that the Dirac point and associated zero-$\bar{k}$ gaps emerge in such a structure, and the positions of zero-$\bar{k}$ gaps and the defect mode are robust against the lattice constant and incident angle. We believe that the analytical and numerical results may lead to promising applications in graphene-based electronic filters and modulators.

References

[1] Novoselov K S, Geim A K, Morozov S V, Jiang D, Zhang Y, Dubonos S V, Grigorieva I V and Firsov A A 2004 *Science* **306** 666

[2] Castro Neto A H, Guinea F, Peres N M R, Novoselov K S and Geim A K 2009 *Rev. Mod. Phys.* **81** 109

[3] Sun L F, Dong L M and Fang C 2013 *Chin. Phys. B* **22** 047203

[4] Sun L F, Dong L M, Wu Z F and Fang C 2013 *Chin. Phys. B* **22** 077201

[5] Miao F, Wijeratne S, Zhang Y, Coskun U C, Bao W and Lau C N 2007 *Science* **317** 1530

[6] Wang F, Zhang Y, Tian C, Girit C, Zettl A, Crommie M and Shen Y R 2008 *Science* **320** 206

[7] Novoselov K S, Geim A K, Morozov S V, Jiang D, Katsnelson M I, Grigorieva I V, Dubonos S V and Firsov A A 2005 *Nature* **438** 197

[8] Purewal M S, Zhang Y and Kim P 2006 *Phys. Status Solidi B* **243** 3418

[9] Kuzmenko A B, van Heumen E, Carbone F and van der Marel D 2008 *Phys. Rev. Lett.* **100** 117401

[10] Bai C and Zhang X 2007 *Phys. Rev. B* **76** 075430

[11] Park C H, Yang L, Son Y W, Cohen M L and Louie S G 2008 *Nat. Phys.* **4** 213

[12] Barbier M, Peeters F M, Vasilopoulos P and Pereira J M Jr 2008 *Phys. Rev. B* **77** 115446

[13] Zhang H Y, Zhang Y P, Gao Y and Yin Y H 2012 *Chin. Phys. Lett.* **29** 128401

[14] Ramezani Masir M, Vasilopoulos P, Matulis A and Peeters F M 2008 *Phys. Rev. B* **77** 235443

[15] Ghosh S and Sharma M 2009 *J. Phys.: Condens. Matter* **21** 292204

[16] Wang S X, Li Z W, Liu J J and Li Y X 2011 *Chin. Phys.* B **20** 077305

[17] Wang L G and Zhu S Y 2010 *Phys. Rev. B* **81** 205444

[18] Wang L G and Chen X 2011 *J. Appl. Phys.* **109** 033710

[19] Guo X X, Liu D and Li Y X 2011 *Appl. Phys. Lett.* **98** 242101

[20] Zhao P L and Chen X 2011 *Appl. Phys. Lett.* **99** 182108

[21] Ma T X, Liang C, Wang L G and Lin H Q 2012 *Appl. Phys. Lett.* **100** 252402

[22] Zhang Y P, Yin Y H , Liu M, Wu Z X, Shen D L, Wang C L and Zhang H Y 2013 *J. Optoelectroni. Laser* **24** 190

[23] Yan W X 2013 *Chin. Phys. Lett.* **30** 047202

[24] Yu X X, Xie Y E, Ou Y T and Chen Y P 2012 *Chin. Phys. B* **21** 107202

[25] Datta S 1995 *Electronic Transport in Mesoscopic Systems* (Cambridge: Cambridge University Press)

[26] Tworzydlo J, Trauzettel B, Titov M, Rycerz A and Beenakker C W J 2006 *Phys. Rev. Lett.* **96** 246802